An analytical model for subsurface irradiance and remote sensing reflectance in deep and shallow case-2 waters

A. Albert
German Aerospace Center (DLR), Remote Sensing Technology Institute, D-82230 Wessling, Germany
andreas.albert@dlr.de

C.D. Mobley
Sequoia Scientific Inc., 2700 Richards Road, Suite 107, Bellevue, WA 98005 USA
mobley@sequoiasci.com

Abstract: Subsurface remote sensing signals, represented by the irradiance reflectance and the remote sensing reflectance, were investigated. The present study is based on simulations with the radiative transfer program Hydrolight using optical properties of Lake Constance (German: Bodensee) based on in-situ measurements of the water constituents and the bottom characteristics. Analytical equations are derived for the irradiance reflectance and remote sensing reflectance for deep and shallow water applications. The input of the parameterization are the inherent optical properties of the water - absorption $a(\lambda)$ and backscattering $b_b(\lambda)$. Additionally, the solar zenith angle θ_s, the viewing angle θ_v , and the surface wind speed u are considered. For shallow water applications the bottom albedo R_B and the bottom depth z_B are included into the parameterizations. The result is a complete set of analytical equations for the remote sensing signals R and R_{rs} in deep and shallow waters with an accuracy better than 4%. In addition, parameterizations of apparent optical properties were derived for the upward and downward diffuse attenuation coefficients K_u and K_d.

OCIS codes: (010.4450) Ocean optics; (010.7340) Water; (280.0280) Remote sensing

References and links

1. H.J. Gordon, O.B. Brown, and M.M. Jacobs, "Computed relationships between the inherent and apparent optical properties of a flat homogeneous ocean," Appl. Opt. **14**, 417-427 (1975).
2. L. Prieur, *Transfers radiatifs dans les eaux de mer*, PhD thesis (Doctorat d'Etat, Univ. Pierre et Marie Curie, Paris, 1976).
3. H.R. Gordon and A.Y. Morel, *Remote assessment of ocean color for interpretation of satellite visible imagery: a review* (Springer, New York, 1983), Vol. 4.
4. H.R. Gordon, O.B. Brown, R.H. Evans, J.W. Brown, R.C. Smith, K.S. Baker, and D.K. Clark, "A semianalytic radiance model of ocean color", J. Geoph. Res. **93**, 10909-10924 (1988).
5. J.T.O. Kirk, "Dependence of relationship between inherent and apparent optical properties of water on solar altitude," Limnol. Oceanogr. **29**, 350-356 (1984).
6. S. Sathyendranath and T. Platt, "Analytic model of ocean color," Appl. Opt. **36**, 2620-2629 (1997).
7. A.G. Dekker, H.J. Hoogenboom, L.M. Goddijn, and T.J.M. Malthus, "The relation between inherent optical properties and reflectance spectra in turbid inland waters," Rem. Sens. Rev. **15**, 59-74 (1997).
8. T. Heege, *Flugzeuggestützte Fernerkundung von Wasserinhaltsstoffen im Bodensee*, PhD thesis (Remote Sensing Technology Institute, German Aerospace Center DLR, 2000).

#3022 - $15.00 US
Received September 17, 2003; Revised October 23, 2003

9. T.T. Bannister, "Model of the mean cosine of underwater radiance and estimation of underwater scalar irradiance," Limnol. Oceanogr. **37**, 773-780 (1992).
10. D.R. Lyzenga, "Passive remote sensing techniques for mapping water depth and bottom features," Appl. Opt. **17**, 379-383 (1978).
11. J. Joseph, "Untersuchungen über Ober- und Unterlichtmessungen im Meere und über ihren Zusammenhang mit Durchsichtigkeitsmessungen," Dt. Hydrogr. Z. **3**, 324-335 (1950).
12. W.D. Philpot and S.G. Ackleson, "Remote sensing of optically shallow, vertically inhomogeneous waters: a mathematical model", Delaware Sea Grant Collage Program (DEL-SG-12-81), 283-299 (1981).
13. S. Maritorena, A. Morel, and B. Gentili, "Diffuse reflectance of oceanic shallow waters: influence of water depth and bottom albedo", Limnol. Oceanogr. **39**, 1689-1703 (1994).
14. T. Ohde and H. Siegel, "Correction of bottom influence in ocean colour satellite images of shallow water areas of the Baltic Sea," Int. J. Rem. Sens. **22**, 297-313 (2001).
15. Z. Lee, K.L. Carder, C.D. Mobley, R.G. Steward, and J.S. Patch, "Hyperspectral remote sensing for shallow waters. 1. A semianalytical model," Appl. Opt. **37**, 6329-6338 (1998).
16. Z. Lee, K.L. Carder, C.D. Mobley, R.G. Steward, and J.S. Patch, "Hyperspectral remote sensing for shallow waters: 2. Deriving bottom depths and water properties by optimization," Appl. Opt. **38**, 3831-3843 (1999).
17. C.D. Mobley, B. Gentili, H.R. Gordon, Z. Jin, G.W. Kattawar, Á. Morel, P. Reinersman, K. Stamnes, and R.H. Stavn, "Comparison of numerical models for computing underwater light fields," Appl. Opt. **32**, 7484-7504 (1993).
18. C.D. Mobley, *Light and water - radiative transfer in natural waters* (Academic Press, San Diego, 1994).
19. P. Gege, "Characterization of the phytoplankton in Lake Constance for classification by remote sensing," Arch. Hydrobiol. Adv. Limnol. **53**, 179-193 (1998).
20. H. Buiteveld, J.H.M. Hakvoort, and M. Donze, "The optical properties of pure water," in *Ocean Optics XII*, Proc. SPIE 2258, 174-183 (1994).
21. A. Bricaud, A. Morel, and L. Prieur, "Absorption by dissolved organic matter of the sea (yellow substance)in the UV and visible domains," Limnol. Oceanogr. **26**, 43-53 (1981).
22. P. Gege, *Lake Constance: yellow substance measurements in 1998* Technical Report (Remote Sensing Technology Institute for Optoelectronics, German Aerospace Center DLR, 1999).
23. T.J. Petzold, *Volume scattering functions for selected ocean waters* (Dowden, Hutchinson & Ross, Stroudsberg, 1977), pp. 152-174.
24. D. Pozdnyakov, A. Lyaskovsky, H. Grassl, and L. Pettersson, "Numerical modelling of transspectral processes in natural waters: implications for remote sensing," Int. J. Rem. Sens. **23**, 1581-1607 (2002).
25. S.K. Hawes, K.L. Carder, and G.R. Harvey, "Quantum fluorescence efficiencies of fulvic and humic acids: effects on ocean color and fluorometric detection," in *Ocean Optics XI*, Proc. SPIE 1750,, 212-223 (1992).
26. T. Heege (Remote Sensing Technology Institute, German Aerospace Center DLR, Personal communication, 2003).
27. K. Bochter and C. Wallhäußer, "New instrument for simultaneous measurement of the daylight field's optical properties above and under water," in *Ocean Optics XIII*, Proc. SPIE 2963, 631-636 (1997).
28. W.W. Gregg and K.L. Carder, "A simple spectral solar irradiance model for cloudless maritime atmospheres," Limnol. Oceanogr. **35**, 1657-1675 (1990).
29. C. Cox and W. Munk, "Statistics of the sea surface derived from sun glitter," J. Mar. Res. **13**, 198-227 (1954).
30. C. Cox and W. Munk, "Measurement of the roughness of the sea surface from photographs of the sun's glitter," J. Opt. Soc. Am. **44**, 838-850 (1954).
31. H.R. Gordon, "Can the Lambert-Beer law be applied to the diffuse attenuation coefficient of ocean water?," Limnol. Oceanogr. **34**, 1389-1409 (1989).
32. J.T.O. Kirk, "The upwelling light stream in natural waters," Limnol. Oceanogr. **34**, 1410-1425 (1989).

1. Introduction

The concentration of water constituents can be derived by optical remote sensing making use of the spectral shape of the reflected sunlight. The models of [1], [2], or [3] for the irradiance reflectance and remote sensing reflectance, R and R_{rs}, use as parameters the absorption $a(\lambda)$ and backscattering coefficient $b_b(\lambda)$:

$$R_\infty = f^\circ \frac{b_b}{a+b_b} \equiv f^\circ x \tag{1}$$

$$R_{rs,\infty} = f^\uparrow \frac{b_b}{a+b_b} \equiv f^\uparrow x = \frac{f^\circ}{Q} x \tag{2}$$

#3022 - $15.00 US Received September 17, 2003; Revised October 23, 2003

The equations are valid just below the water surface. The higher the backscattering, the higher the reflectance and the higher the absorption, the lower the reflectance. f° is the proportionality factor for the irradiance reflectance and $f^{\uparrow}$ for the remote sensing reflectance of an infinitely deep water body (index ∞). The Q-factor is defined as the ratio of the upwelling irradiance and the upwelling radiance: $Q = \frac{E_u}{L_u}$. For an isotropic upwelling radiance distribution, $Q = \pi$ sr. Thus, the Q-factor is a measure of the anisotropy of the light field distribution. In natural waters, Q is typically around 5 sr. Using the definitions of the irradiance reflectance and remote sensing reflectance, $R = \frac{E_u}{E_d}$ and $R_{rs} = \frac{L_u}{E_d}$, the Q-factor is also the ratio of the irradiance reflectance to the remote sensing reflectance according to Eq. (2).

These approximations are valid for infinitely deep water, where only the water body contributes to the reflected signal. For open ocean case-1 waters, constant proportionality factors are commonly used and are sufficient for many applications, for example $f^{\circ} = 0.33$ [1] and $f^{\uparrow} = 0.095$ [4]. Due to the influences of the sun and surface geometry on the reflectances, a parameterization of the factors can be developed including these aspects and the inherent optical properties as well [5, 6]. But in case-2 waters, the factors f° and $f^{\uparrow}$ are not constant and can vary in time and location [7]. [8] used for his determination at Lake Constance (German: Bodensee) a combination of the model of [5] and [9].

In addition, if remote sensing data are analyzed including optically shallow waters, the bottom depth z_B and the bottom albedo R_B have to be taken into account [10]. Following [11], different authors including [12], [13], or [14] have formulated approximations of the irradiance reflectance for shallow water. Their equations result from a two-flow irradiance approximation including the bottom influences:

$$R = R_{\infty}\left(1 - \mathrm{e}^{-2Kz_B}\right) + R_B \mathrm{e}^{-2Kz_B}$$

K is the diffuse attenuation coefficient of the water column and is equal for the downward and upward directions. According to [15], this equation can be transformed to the remote sensing reflectance R_{rs} as follows:

$$R_{rs} = R_{rs,\infty}\left(1 - \mathrm{e}^{-2Kz_B}\right) + \frac{R_B}{\pi}\mathrm{e}^{-2Kz_B}$$

However, in reality the diffuse attenuation coefficients of the upwelling and downwelling light are not equal. To get a more accurate expression the effective attenuation coefficient is divided into an upwelling and a downwelling part. The upwelling part distinguishes between radiation reflected in the water column (index W) and from the bottom (index B). This results in the following equations, as mentioned in [15] and [16]:

$$R = R_{\infty}\left(1 - \mathrm{e}^{-(K_d + K_{u,W})z_B}\right) + R_B \mathrm{e}^{-(K_d + K_{u,B})z_B} \tag{3}$$

$$R_{rs} = R_{rs,\infty}\left[1 - \exp\left\{-\left(K_d + \frac{K_{u,W}}{\cos\theta_v}\right)z_B\right\}\right] + \frac{R_B}{\pi}\exp\left\{-\left(K_d + \frac{K_{u,B}}{\cos\theta_v}\right)z_B\right\} \tag{4}$$

The viewing angle just below the water surface, θ_v, is included in Eq. (4) in the upward attenuation due to the dependence of the upwelling radiance on the viewing position.

Based on these equations new analytical parameterizations were developed for the reflectances of deep and shallow water, the upwelling, and the downwelling attenuation coefficients to obtain an invertable equation for remote sensing data. Simulations were made with the well-established and validated radiative transfer program Hydrolight (version 3.1) [17, 18] for case-2 waters and the results fitted to Eq. (3) and (4). The program code was optimized for

#3022 - $15.00 US Received September 17, 2003; Revised October 23, 2003

the test site Lake Constance, located in southern Germany at the borders with Switzerland and Austria. The optical properties of Lake Constance were investigated by [19] and [8] and were included into the source code of Hydrolight. The simulations with Hydrolight were performed not only over the natural range of the concentrations of the water constituents found for Lake Constance, but also below and above this range to cover a more general range of concentrations. This extends the validity of the developed parameterizations for a wide number of case-2 waters.

2. Radiative transfer model

For the forward simulation of the underwater light field the radiative transfer program Hydrolight (version 3.1) was used. The model is explained in detail by [17] and [18]. The optical properties are selected for case-2 waters, such as the test site at Lake Constance, and are given for three kinds of water constituents: phytoplankton (index P), suspended matter (index X), and gelbstoff (index Y). Gelbstoff is also known as Colored Dissolved Organic Matter (CDOM), yellow substance, or gilvin. Thus, the total absorption and backscattering coefficients, $a(\lambda)$ and $b_b(\lambda)$, are the sums of all contributions of each water constitutent and pure water (index W) itself:

$$\begin{aligned} a(\lambda) &= a_W(\lambda) + a_P(\lambda) + a_X(\lambda) + a_Y(\lambda) \\ b_b(\lambda) &= b_{b,W}(\lambda) + b_{b,P}(\lambda) + b_{b,X}(\lambda) + b_{b,Y}(\lambda) \end{aligned}$$

Due to the symmetric scattering properties of water, the backscattering coefficient of pure water can be determined from the scattering coefficient b_W: $b_{b,W} = \frac{1}{2} b_W$. The absorption $a_W(\lambda)$ and scattering coefficient $b_W(\lambda)$ of pure water are taken from [20]. The absorption and backscattering coefficients of phytoplankton and suspended matter are the product of the specific absorption and backscattering coefficients and the concentrations. The specific absorption of phytoplankton $a_P^*(\lambda)$ is given after [8] by the mean value of measurements of [19] at Lake Constance. Absorption of suspended matter was investigated for Lake Constance by [8]. He found no specific absorption and therefore a_X is set to zero. The absorption of gelbstoff is approximated by an exponential function [21] with an exponent $S = 0.014$ nm^{-1} at a reference wavelength λ_0 of 440 nm after [22]. The scattering in the water is mainly driven by the amount of suspended matter. The influence of the particulate fraction of phytoplankton on the scattering is included in the value of the scattering and backscattering coefficients of suspended matter as investigated by [8] and therefore, $b_{b,P} = 0$. There was also no dependence of the scattering and backscattering coefficients found at the wavelengths between 400 and 800 nm. Hence, the constant value of the specific backscattering coefficient of suspended matter $b_{b,X}^* = 0.0086$ m^2/g obtained for Lake Constance was used. The ratio of the specific scattering to backscattering coefficient is 0.019 [8], which is the same as found by [23] in San Diego harbor. Therefore, this phase function was chosen for all simulations. Gelbstoff is assumed not to scatter light because its pigments are totally dissolved in the water. Finally, the following equations are obtained for the absorption and the backscattering coefficients:

$$a(\lambda) = a_W(\lambda) + a_P^*(\lambda) C_P + a_Y(\lambda_0) \mathrm{e}^{-S(\lambda - \lambda_0)} \quad (5)$$

$$b_b(\lambda) = \frac{1}{2} b_W(\lambda) + b_{b,X}^* C_X \quad (6)$$

C_P is the concentration of phytoplankton, which is given as the sum of chlorophyll-a and phaeophytin-a concentration in units of μg/l. C_X is the concentration of suspended matter in units of mg/l.

The impact of inelastic processes in natural water was recently investigated by [24] and found to contribute significantly to the irradiance reflectance and remote sensing reflectance. Hence,

#3022 - $15.00 US Received September 17, 2003; Revised October 23, 2003

the fluorescence of chlorophyll and gelbstoff as well as Raman scattering were included in all simulations using the default efficiencies of Hydrolight (version 3.1). The quantum efficiency of chlorophyll fluorescence was set to 2% and the emission function was approximated by a Gaussian function centered at the wavelength 685 nm with 10.6 nm full width at half maximum. The fluorescence of gelbstoff was described by the spectral fluorescence quantum efficiency function defined by [25] between 310 and 490 nm. The quantum efficiency took values of about 0.9 to 1.9% in this wavelength interval. The Raman scattering was approximated using a wavenumber redistribution function expressed by the sum of four Gaussian functions representing the number of shifts for a scattered photon. For more details see [18].

The water constituents are in general not homogeneously distributed with depth in natural waters. Thus, to match on average the real situations of the test site Lake Constance, depth profiles of the water constituents were included in all the simulations. More than 500 depth profiles were measured at Lake Constance between 1986 and 1996. The data were analyzed and mean profiles were determined for phytoplankton and suspended matter [8, 26]. The minimum concentration of phytoplankton was 1.0 μg/l used for determining the depth profile. The dependence of the concentration on the depth z can be expressed as

$$C(z) = C_0 + C_{max} \exp\left\{-\frac{1}{2}\left(\frac{|z - z_{max}|}{\sigma}\right)^n\right\} \tag{7}$$

where $C(z)$ is the concentration of phytoplankton or suspended matter. For gelbstoff, no depth dependence was found. The values of the coefficients C_0, z_{max}, σ, and n are listed in table 1. If, for example, a constant value of the concentration for all depths is used, the irradiance reflectance is underestimated by 12 to 15% for concentrations of 2 to 5 μg/l phytoplankton and 2 to 5 mg/l suspended matter.

Table 1. Values of the constant factors of phytoplankton and suspended matter for the depth profile in Eq. (7).

	C_0	z_{max} (m)	σ (m)	n
Phytoplankton	1.0 μg/l	2.9	9.6	3.0
Suspended matter	0.9 mg/l	12.9	10.7	2.3

For the simulations from 400 to 750 nm with steps of 5 nm, the concentrations of the water constituents at the surface were varied beyond their natural ranges at Lake Constance (see figures 1 and 2). The values are given in table 2. To get a suitable depth profile for the lowest concentrations of phytoplankton and suspended matter the coefficient C_0 in table 1 was adjusted to 0.5 μg/l and 0.5 mg/l respectively.

Table 2. Concentrations of the water constituents for the simulations with Hydrolight.

C_P (μg/l)	0.5	1.0	1.5	2.0	3.0	5.0	7.0	10.0
	20.0	40.0	60.0	80.0	100.0			
C_X (mg/l)	0.5	1.0	1.5	2.0	3.0	4.0	5.0	6.0
	7.0	9.0	10.0	30.0	50.0			
$a_Y(\lambda_0)(\mathrm{m}^{-1})$	0.05	0.10	0.15	0.20	0.30	0.40	0.50	0.60
	0.70	0.80	0.90	1.00	1.30	2.50	4.00	5.00

#3022 - $15.00 US Received September 17, 2003; Revised October 23, 2003

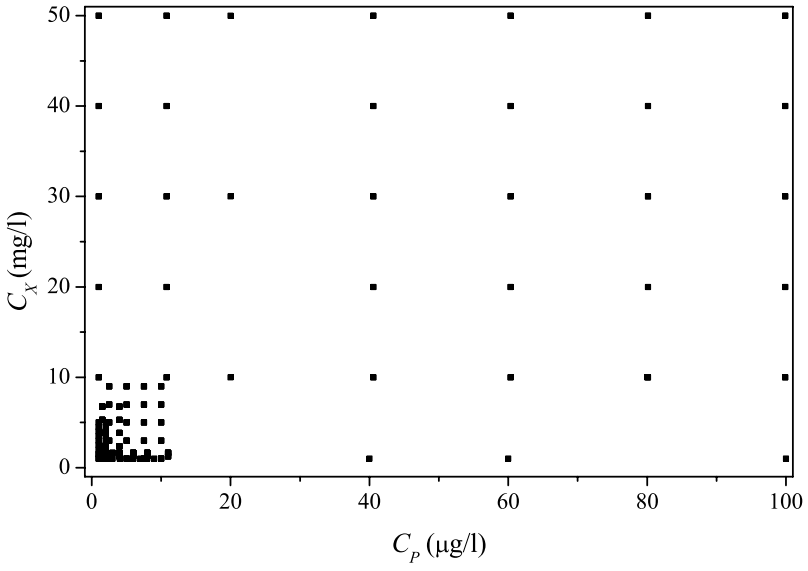

Fig. 1. Distribution of the concentration of suspended matter against phytoplankton for the simulations with Hydrolight.

For the bottom albedo, spectra of sand and green algae included in Hydrolight were used. Additionally, bottom albedo spectra were measured at Lake Constance for sediment and macrophyte covered beds with the Hydrological Spectral Radiometer HYDRA [27]. The sediment was gray colored mud consisting of about 50% inorganic particles and 50% organic matter typically for Lake Constance. The average particle size is around 10 μm. The reflectance of the macrophyte was measured above a patch of the species *Potamogeton Pectinatus* L. with senescent leaves. The bottom reflectances used for the simulations are shown in figure 3. Bottom depth was set to 1, 3, 6, 10, 20, 30 m, and infinitely deep water. For simulating the sun and sky conditions the model of [28] included in Hydrolight was used. Clear sky conditions were chosen with varying subsurface sun zenith angle θ_s. The angles were 8, 14, 21, 27, 34, 39, 43, and 46°. The forward simulations were performed for values of the surface wind speed u of 0, 5, and 10 m/s using the sea surface statistical model incorporated into Hydrolight. This surface representation is based on the wave-slope wind-speed laws of [29, 30] and thus includes both gravity and capillary wave effects.

Altogether, over 1400 spectra were simulated. The output of the Hydrolight simulations is given for different subsurface viewing angles θ_v ranging between 8° and 46° in the same manner as the sun zenith angle.

3. Results

The output of Hydrolight of the irradiance reflectance and remote sensing reflectance, R and R_{rs}, were investigated to find parameterizations for the inherent optical properties as well as for the sun and viewing geometry using Eq. (3) and (4). The unknown variables in these equations are the irradiance reflectance and remote sensing reflectance of the water body, R_∞ and $R_{rs,\infty}$, and the diffuse attenuation coefficients K_d, $K_{u,W}$, and $K_{u,B}$. For each of these unknown

#3022 - $15.00 US
Received September 17, 2003; Revised October 23, 2003

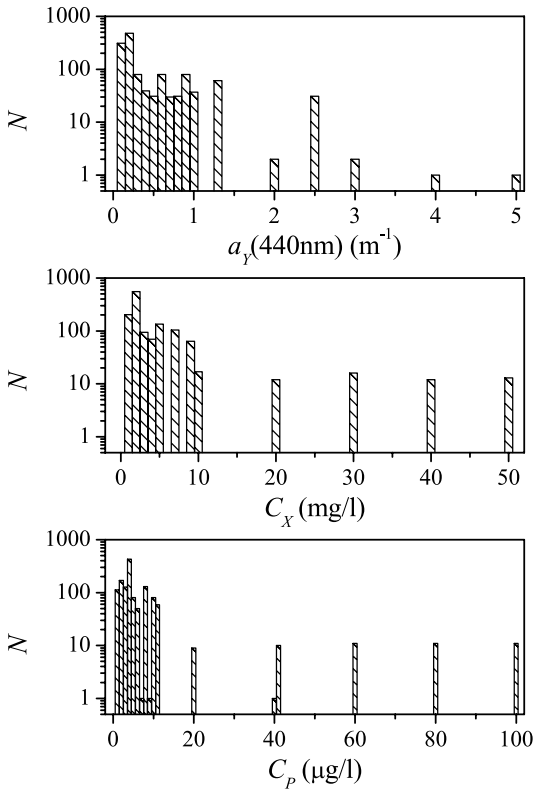

Fig. 2. Distribution of the concentration values of gelbstoff (top), suspended matter (center), and phytoplankton (bottom) for the simulations with Hydrolight.

factors new parameterizations were developed based on the inherent optical properties, the solar and viewing angles, and the surface wind speed. Wavelength dependence was included in the inherent optical properties. For all simulations chlorophyll and gelbstoff fluorescence was considered as mentioned above. For the determination of the parameterizations, wavelengths around the strongly peaked fluorescence emission of chlorophyll from 660 to 715 nm were excluded to give a better spectral fit. The parameterizations were generated by fitting the simulated values using the Levenberg-Marquardt multivariate optimization technique yielding regression coefficients. These regression coefficients allow calculation of the reflectances and attenuation coefficients using analytical equations. The mean relative error $\overline{\delta}$ documents the accuracy of the analytical parameterizations and was estimated by

$$\overline{\delta} = \frac{X - X_0}{X_0} = \frac{\Delta X}{X_0},$$

where X represents the value calculated by the parameterization and X_0 the value of the simulation.

#3022 - $15.00 US
Received September 17, 2003; Revised October 23, 2003

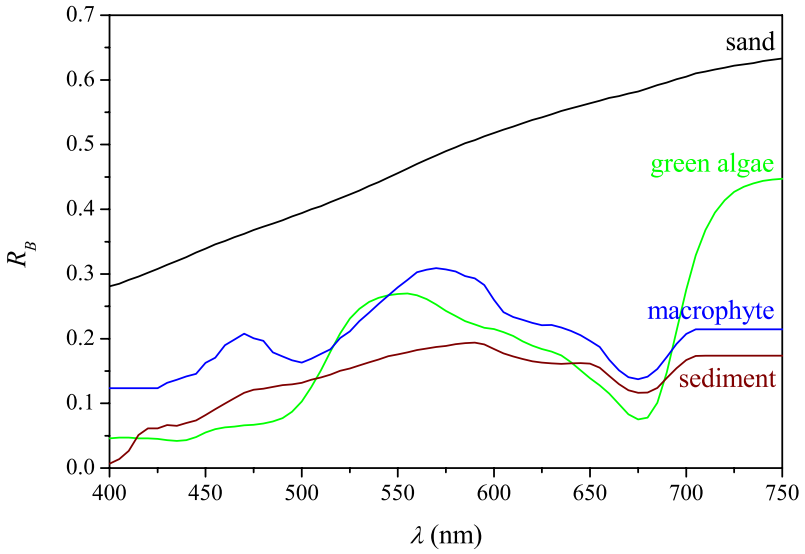

Fig. 3. Bottom reflectance spectra used for the forward simulations in Hydrolight.

3.1. Deep water

3.1.1. Irradiance reflectance

The underwater irradiance reflectance for deep water R_∞ at depth $z = 0$ is parameterized using Eq. (1). The factor f° was analyzed for its dependence on x, u, and θ_s. The simulations yield a non-linear dependence on the factor x (Fig. 4) and the subsurface solar zenith angle θ_s (Fig. 5 right) and a linear dependence on the surface wind u (Fig. 5 left). For the investigation of the dependence on surface wind, additional calculations were made for wind speed values ranging from 0 to 30 m/s in steps of 1 m/s. The following parameterization was found to be suitable:

$$\begin{aligned} R_\infty &= f^\circ(x,\theta_s,u)x = f^\circ(x)f^\circ(\theta_s)f^\circ(u)x \\ &= p_1\left(1+p_2x+p_3x^2+p_4x^3\right)\left(1+p_5\frac{1}{\cos\theta_s}\right)(1+p_6u)x \end{aligned} \tag{8}$$

Using fewer coefficients for the factor x results in a significantly lower correlation. The coefficients p_1 to p_6 were determined using $N = 22184$ model results. The results of the regression are listed in table 3. The errors of using a constant factor f° is illustrated by figure 4. The dashed line corresponds to the value of $f^\circ = 0.33$ by [1]. For high values of x, which means high backscattering or high concentration of suspended matter, the error increases up to 100%. With the new parameterization the error is reduced significantly. Figure 6 shows, on the left hand side, the calculated plotted against the simulated values. The black crosses are the estimated values with Eq. (8) and the blue points are the values derived by the previous model of [8]. The distribution of the relative error $\overline{\delta}$ between the simulated and predicted values of R_∞ with Eq. (8) (Fig. 6 right) shows a normal distribution with a mean value of 0.04 while the mean error using a constant $f^\circ = 0.33$ is -0.25. The new parameterization gives also much better results than models of [5] and [6] which include the sun zenith angle to estimate the factor f° (graph not shown). The previous model of [8] for Lake Constance results in a mean relative error of 0.08

#3022 - $15.00 US Received September 17, 2003; Revised October 23, 2003

(Fig. 6 right). But for irradiance reflectances greater than 20% the mean relative error is 0.22. For these situations of high backscattering due to high amount of suspended matter, the new parameterization results in a mean relative error below 1%.

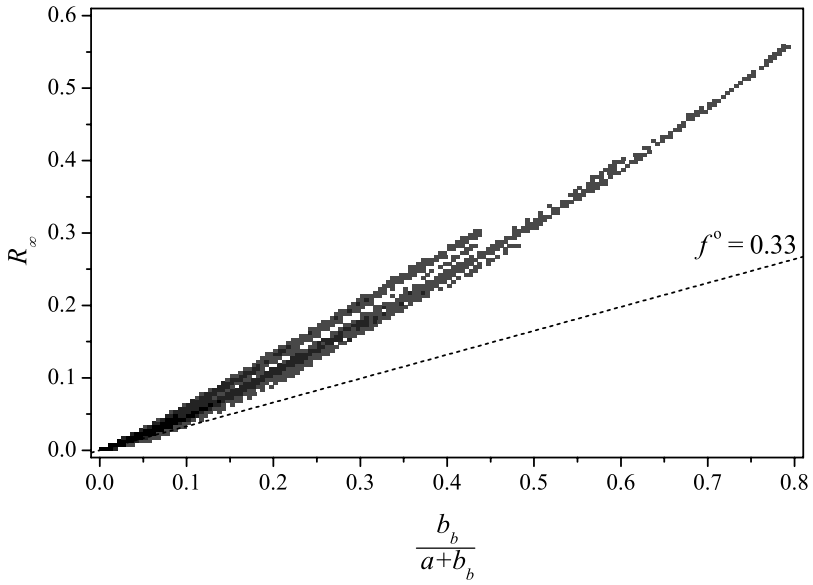

Fig. 4. Irradiance reflectance for infinitely deep water simulated with Hydrolight ($N = 22184$) depending on $x = \frac{b_b}{a+b_b}$ and the approximation of [1] for a factor $f^\circ = 0.33$ (dashed line).

The advantage of the new parameterization is the separation of the dependences on the inherent optical properties and the sun and surface geometry. This allows the influence of the variables on the remote sensing signal to be analyzed separately. The surface wind speed has the weakest influence. If it is neglected, the error is below 1%. The influence of the sun position is greater: the variation of the irradiance reflectance is about 15% for a subsurface solar zenith angle from 0 to 25° and about 30% for 0 to 40°.

3.1.2. Remote sensing reflectance

The determination of the remote sensing reflectance from the irradiance reflectance is possible using the Q-factor, $R_{rs,\infty} = \frac{R_\infty}{Q}$. The Q-factor is determined by the angular distribution of the light field under water. Therefore, a parameterization of $Q = Q(\theta_s, \theta_v, u)$ seemed to be suitable. All data points were analyzed, but no suitable parameterization was found. The reason is that the angular distribution of Q is controlled also significantly by the inherent optical properties and their concentrations: $Q = Q(\theta_s, \theta_v, u, x)$. Thus, an equation for the remote sensing reflectance in deep water was established that is similar to the equation for the irradiance reflectance, but with different values of the coefficients. The factor $f^\uparrow$ is derived as a function of separated variables. In addition to the dependences on x, θ_s, and u the remote sensing reflectance varies with the subsurface viewing angle θ_v. Simulations using different values of θ_v are shown in Fig. 7. The data points can be fitted with a function proportional to $\frac{1}{\cos\theta_v}$. The variation of the remote sensing reflectance is about 10% for a subsurface viewing angle from 0 to 25°. This is

#3022 - $15.00 US Received September 17, 2003; Revised October 23, 2003

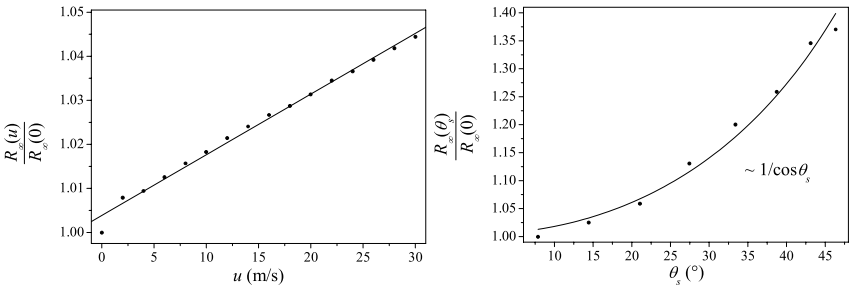

Fig. 5. Dependence of the irradiance reflectance for infinitely deep water on surface wind (left) and subsurface solar zenith angle (right). The concentrations of the water constituents are $C_P = 3$ μg/l, $C_X = 3$ mg/l, and $a_Y(\lambda_0) = 0.2\text{m}^{-1}$.

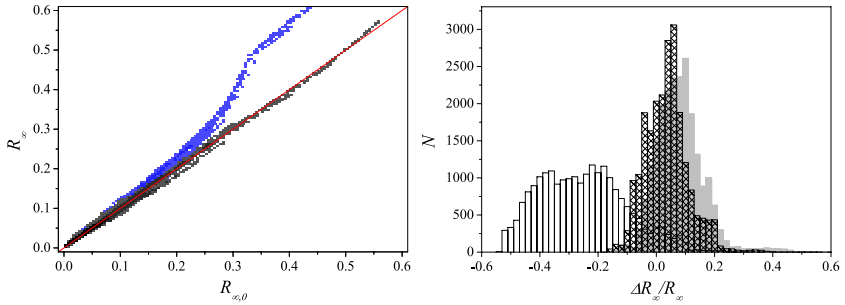

Fig. 6. Left: irradiance reflectance calculated by Eq. (8) (black crosses) and by the model of [8] (blue points) against the simulated values for infinitely deep water. The 1:1 line is plotted in red. Right: distribution of the relative errors for the approximation of [1] (white bars), [8] (gray bars), and of the new parameterization of Eq. (8) (cross hatched bars).

accounted for using the following parameterization:

$$\begin{aligned} R_{rs,\infty} &= f^{\uparrow}(x,\theta_s,u,\theta_v)x = f^{\uparrow}(x)f^{\uparrow}(\theta_s)f^{\uparrow}(u)f^{\uparrow}(\theta_v)x \\ &= p_1\left(1+p_2x+p_3x^2+p_4x^3\right) \\ &\quad\times\left(1+p_5\frac{1}{\cos\theta_s}\right)(1+p_6u) \\ &\quad\times\left(1+p_7\frac{1}{\cos\theta_v}\right)x \end{aligned} \tag{9}$$

The results of the regression are listed in table 3. $N = 177472$ model results were used to calculate the coefficients of the equation. Figure 8 shows the calculated values plotted against the simulated. The mean relative error is about 0.02.

Received September 17, 2003; Revised October 23, 2003

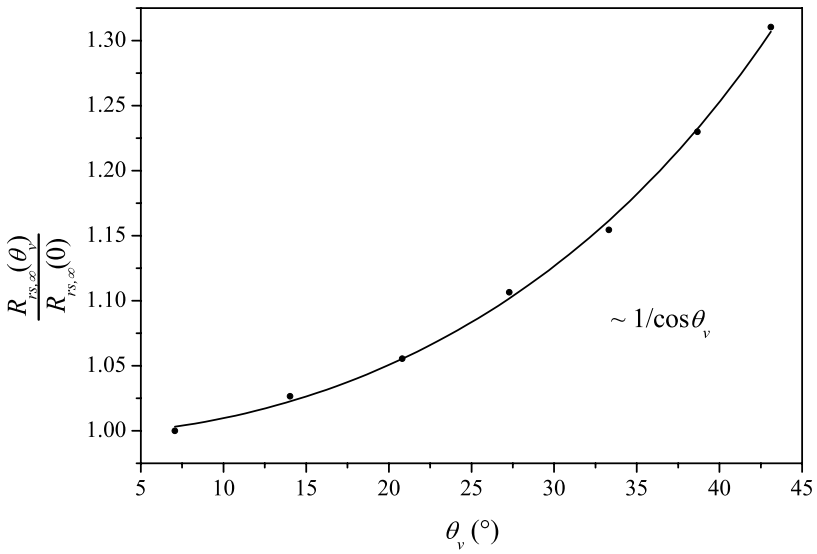

Fig. 7. Dependence of the remote sensing reflectance for infinitely deep water on the subsurface viewing angle θ_v. The concentrations of the water constituents are $C_P = 3$ μg/l, $C_X = 3$ mg/l, and $a_Y(\lambda_0) = 0.2\text{m}^{-1}$.

Table 3. Coefficients for the irradiance reflectance of deep water for Eq. (8) and for the remote sensing reflectance of deep water for Eq. (9).

	R_∞ of Eq. (8)	$R_{rs,\infty}(\text{sr}^{-1})$ of Eq. (9)
p_1	0.1034 ± 0.0014	0.0512 ± 0.0001 sr^{-1}
p_2	3.3586 ± 0.0305	4.6659 ± 0.0174
p_3	-6.5358 ± 0.0808	-7.8387 ± 0.0434
p_4	4.6638 ± 0.0649	5.4571 ± 0.0345
p_5	2.4121 ± 0.0443	0.1098 ± 0.0018
p_6 (s/m)	-0.0005 ± 0.0001	-0.0044 ± 0.0000
p_7	-	0.4021 ± 0.0020

3.2. Diffuse attenuation coefficient

The reflectances of deep water are the input for the shallow water Eq. (3) and (4). To employ these equations it is necessary to estimate the diffuse attenuation coefficients. The diffuse attenuation describes the loss of up- and downwelling irradiance within a thin layer in the water. This loss depends on absorption, scattering, and the isotropy of the light field. The latter is parameterized by the mean cosine $\overline{\mu}$. For a totally isotropic light distribution $\overline{\mu}$ is 0 and for a collimated beam in direction θ the mean cosine has the value $\overline{\mu} = \cos\theta$ (see [18] for example). In clear sky conditions, just below the water surface the distribution of the light is mainly affected by the direct beam of the sun. Thus, the mean cosine is approximately the cosine of the subsurface solar zenith angle θ_s in the upper water layers.

#3022 - $15.00 US
Received September 17, 2003; Revised October 23, 2003

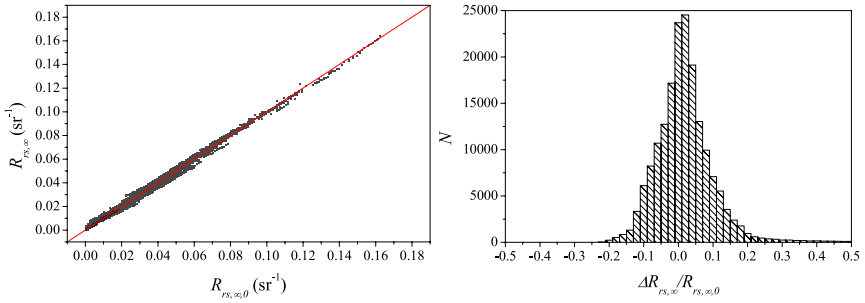

Fig. 8. Left: remote sensing reflectance calculated by Eq. (9) against the simulated values for infinitely deep water. The 1:1 line is plotted in red. Right: distribution of the relative errors.

3.2.1. Downward diffuse attenuation

K_d depends on the absorption and backscattering as well as on the solar zenith angle as shown in figure 9 (left). After [31], the parameterization for K_d is

$$K_d = \kappa_0 \frac{a + b_b}{\cos\theta_s} \tag{10}$$

The simulated values of K_d range from about 0.1 m^{-1} to 10.6 m^{-1} with a mean value of 0.7 m^{-1}. The regression of $N = 72558$ data points gives a value of $\kappa_0 = 1.0546 \pm 0.0001$. The mean relative error is $\overline{\delta} = -0.01$. The distribution of the relative errors is shown in figure 9 (right).

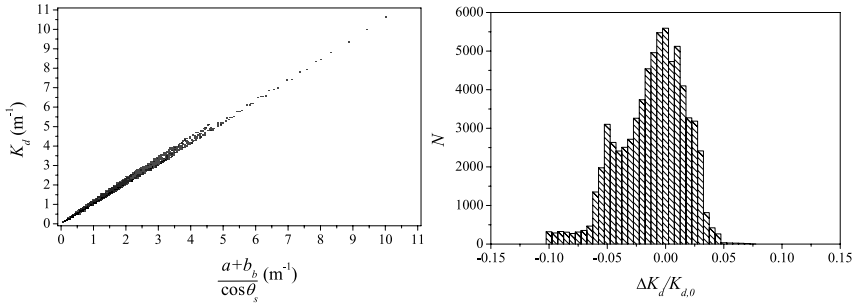

Fig. 9. Downward diffuse attenuation coefficient of 72558 simulations with Hydrolight. Left: dependency on $\frac{a+b_b}{\cos\theta_s}$. Right: distribution of the relative errors between calculated and simulated values.

3.2.2. Upward diffuse attenuation

The investigation on the upwelling diffuse attenuation coefficient is first done for the infinitely deep water body to find the best parameterization. Figure 10 shows the dependence of K_u on

#3022 - $15.00 US Received September 17, 2003; Revised October 23, 2003

absorption and backscattering (left) and on the subsurface solar zenith angle (right). The graph on the right hand side indicates the following dependence of K_u on the subsurface solar zenith angle θ_s: $K_u \propto \frac{1}{\cos\theta_s}$. On the left hand side the dependence on absorption and backscattering is plotted. The colors indicate the concentration of suspended matter C_X which is directly linked to the backscattering coefficient as described in Eq. (6). Generally, a linear dependence on the sum of absorption and backscattering can be assumed: $K_u \propto (a+b_b)$. However, for concentrations of suspended matter of $C_X < 3.0$ mg/l the relationship differs increasingly from a linear dependence. The upward diffuse attenuation coefficient takes higher values for a lower amount of scattering particles in the water. This is because few photons are scattered upwards, resulting in an anisotropic light field [32]. To correct for this effect an additional term is included depending on $x = \frac{b_b}{a+b_b}$. The following equation for the upward diffuse attenuation coefficient shows the best fit when used in Eq. (3) and (4).

$$K_u = (a+b_b)(1+x)^{\kappa_1}\left(1+\kappa_2\frac{1}{\cos\theta_s}\right) \tag{11}$$

For the simulations of an infinitely deep water body the mean relative error was $\overline{\delta} = 0.13$ for $N = 22184$ points. To separate the influence of photons reflected by the water column and the bottom, two different upward diffuse attenuation coefficients, $K_{u,W}$ and $K_{u,B}$, are used for shallow water applications. Thus, four coefficients $\kappa_{i,W}$ and $\kappa_{i,B}$ with $i = 1,2$ were determined by fitting the entire Eq. (3) and (4). The results of the regression are given in table 4. Since the output of Hydrolight is the total upward diffuse attenuation coefficient, which is not the sum of $K_{u,W}$ and $K_{u,B}$, no mean relative errors can be specified.

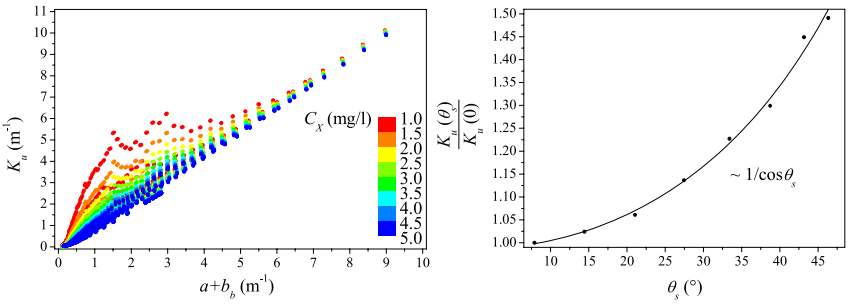

Fig. 10. Dependency of the upward diffuse attenuation coefficient on the sum of absorption and backscattering (left) and subsurface solar zenith angle (right). The points on the left are for $\theta_s = 8^\circ$ with colors representing the concentration of suspended matter and the curve on the right is for $C_P = 1$ μg/l, $C_X = 1$ mg/l, and $a_Y(\lambda_0) = 0.2\text{m}^{-1}$.

3.3. Shallow water

Putting all the above results together the shallow water reflectances can be calculated using Eq. (3) and (4). Additional coefficients A_1 and A_2 are introduced to adapt the equations to the simulated situations.

#3022 - $15.00 US
Received September 17, 2003; Revised October 23, 2003

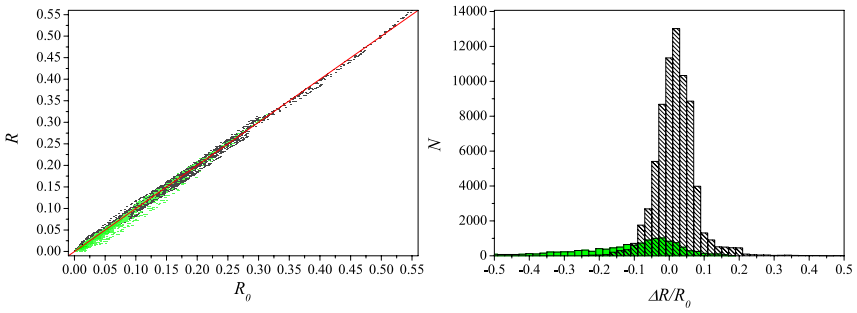

Fig. 11. Irradiance reflectance of shallow water. Comparison of simulated values R_0 and estimated values R (left) with the 1:1 line in red; the green points are the values for wavelengths from 660 to 715 nm. Distribution of the relative error between simulated and estimated irradiance reflectances.

3.3.1. Irradiance reflectance

With the new parameterizations of the diffuse attenuation coefficients and the factors A_1 and A_2, the irradiance reflectance can be expressed by

$$\begin{aligned} R &= R_\infty \left[1 - A_1 \exp\left\{ -\left(\frac{\kappa_0}{\cos\theta_s} + (1+x)^{\kappa_{1,W}} \left(1 + \frac{\kappa_{2,W}}{\cos\theta_s} \right) \right) (a+b_b) z_B \right\} \right] \\ &+ A_2 R_B \exp\left\{ -\left(\frac{\kappa_0}{\cos\theta_s} + (1+x)^{\kappa_{1,B}} \left(1 + \frac{\kappa_{2,B}}{\cos\theta_s} \right) \right) (a+b_b) z_B \right\} \end{aligned} \tag{12}$$

The values of A_1 and A_2 were determined by fitting $N = 72558$ simulated data points. The resulting coefficients are listed in Table 4. In Fig. 11 the estimated irradiance reflectance, R, is plotted against the simulated reflectance, R_0, for all cases. The distribution of the relative error - with a mean error of $\overline{\delta} = 0.02$ - is also shown in Fig. 11. For comparison, the original Eq. (3) of [13] using Eq. (8) for the irradiance reflectance of the water column gives a relative mean error of $\overline{\delta} = 0.06$.

The green points in Figure 11 are the values for wavelengths from 660 to 715 nm. Although these wavelengths were excluded for algorithm development due to the influence of chlorophyll fluorescence, the estimation with Eq. (12) using the parameters of Table 4 is in fair agreement with the simulated values. The mean relative error for these wavelengths is $\overline{\delta} = -0.12$. This means that the new parameterization can be applied also to these wavelengths with an underestimation of about 12%.

The spectral shape of three examples is shown in Fig. 12 in a range from 400 to 750 nm with the relative errors compared to the simulations of Hydrolight. The numbers in the figure correspond to the following conditions:

1. Bottom type is sediment at a depth of $z_B = 5$ m; the concentration of the water constituents are phytoplankton $C_P = 10.8$ μg/l, suspended matter $C_X = 50.0$ mg/l, and gelbstoff $a_Y(440\text{nm}) = 0.2$ m^{-1}; the subsurface solar zenith angle is $\theta_s = 27°$; the wind speed is $u = 1$ m/s.

2. Macrophytes at $z_B = 6$ m; $C_P = 2.5$ μg/l, $C_X = 7.0$ mg/l, and $a_Y(440\text{nm}) = 0.3$ m^{-1}; $\theta_s = 33°$; $u = 0$ m/s.

#3022 - $15.00 US Received September 17, 2003; Revised October 23, 2003

3. Sediment at $z_B = 5$ m; $C_P = 1.0$ μg/l, $C_X = 1.0$ mg/l, and $a_Y(440\text{nm}) = 0.05$ m^{-1}; $\theta_s = 27^\circ$; $u = 1$ m/s.

The agreement between simulation and calculation with Eq. (12) is very good in each case. The relative error (Fig. 12: right) is below 5% over the entire spectral range, except for wavelengths around 685 nm. This is due to the fluorescence of chlorophyll which is not parameterized in these analytical equations. The differences in the other parts of the spectra are mainly caused by the fluorescence of gelbstoff which affects mostly the green part of the visible spectrum [24].

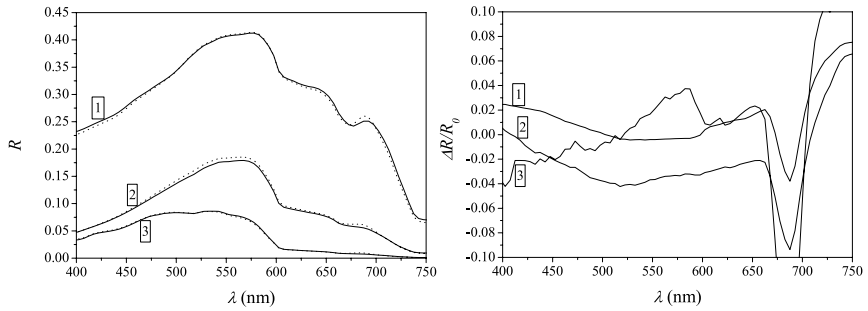

Fig. 12. Irradiance reflectance of shallow water for the spectral range from 400 to 750 nm for three different cases. Left: comparison of simulated (dotted lines) and estimated values (solid lines); right: relative errors. The numbers refer to the following situations: (1) sediment at $z_B = 5$ m, $C_P = 10.8$ μg/l, $C_X = 50.0$ mg/l, $a_Y(440\text{nm}) = 0.2$ m^{-1}, $\theta_s = 27^\circ$, $u = 1$ m/s; (2) macrophytes at $z_B = 6$ m, $C_P = 2.5$ μg/l, $C_X = 7.0$ mg/l, $a_Y(440\text{nm}) = 0.3$ m^{-1}, $\theta_s = 33^\circ$, $u = 0$ m/s; (3) sediment at $z_B = 5$ m, $C_P = 1.0$ μg/l, $C_X = 1.0$ mg/l, $a_Y(440\text{nm}) = 0.05$ m^{-1}, $\theta_s = 27^\circ$, $u = 1$ m/s.

3.3.2. Remote sensing reflectance

The remote sensing reflectance R_{rs} can be expressed with a similar approximation as the irradiance reflectance, but with an additional dependence on the subsurface viewing angle θ_v.

$$\begin{aligned} R_{rs} &= R_{rs,\infty}\left[1 - A_1 \exp\left\{-\left(\kappa_0 \frac{\cos\theta_v}{\cos\theta_s} + (1+x)^{\kappa_{1,W}}\left(1 + \frac{\kappa_{2,W}}{\cos\theta_s}\right)\right)\frac{a+b_b}{\cos\theta_v} z_B\right\}\right] \\ &+ A_2 \frac{R_B}{\pi} \exp\left\{-\left(\kappa_0 \frac{\cos\theta_v}{\cos\theta_s} + (1+x)^{\kappa_{1,B}}\left(1 + \frac{\kappa_{2,B}}{\cos\theta_s}\right)\right)\frac{a+b_b}{\cos\theta_v} z_B\right\} \end{aligned} \quad (13)$$

The results of the regression analysis of $N = 580464$ numbers of observations are listed in Table 4 below. Figure 13 shows the estimated against the simulated values and the relative error, with a mean error of $\overline{\delta} = 0.03$. For comparison, the equation of [15] gives a relative mean error of -0.09.

As mentioned for the case of the irradiance reflectance, the green points in Fig. 13 are the values for wavelengths from 660 to 715 nm. The correlation between the estimated and simulated values are very good here as well. The mean relative error for these wavelengths is $\overline{\delta} = -0.13$. This means that the new parameterization can be applied also to these wavelengths with an underestimation of about 13%.

#3022 - $15.00 US
Received September 17, 2003; Revised October 23, 2003

Table 4. Coefficients for the irradiance and remote sensing reflectance of Eq. (12) and (13) for shallow water.

	R of Eq. (12)	$R_{rs}(\mathrm{sr}^{-1})$ of Eq. (13)
A_1	1.0546 ± 0.0038	1.1576 ± 0.0014
κ_0	1.0546 ± 0.0001	1.0546 ± 0.0001
$\kappa_{1,W}$	1.9991 ± 0.0305	3.5421 ± 0.0152
$\kappa_{2,W}$	0.2995 ± 0.0122	-0.2786 ± 0.0030
A_2	0.9755 ± 0.0013	$1.0389 \pm 0.0004\ \mathrm{sr}^{-1}$
$\kappa_{1,B}$	1.2441 ± 0.0209	2.2658 ± 0.0076
$\kappa_{2,B}$	0.5182 ± 0.0036	0.0577 ± 0.0009

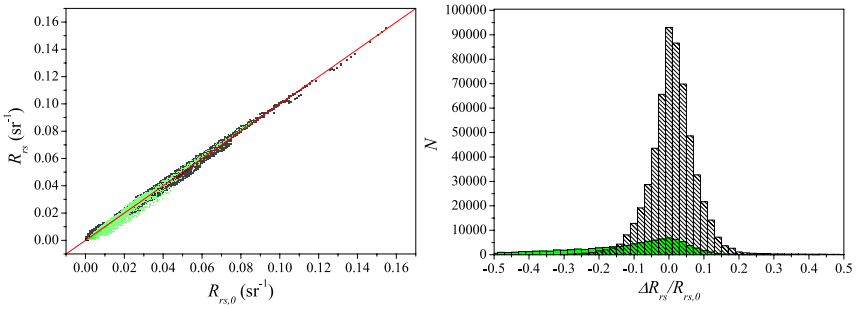

Fig. 13. Remote sensing reflectance of shallow water. Comparison of simulated values $R_{rs,0}$ and estimated values R_{rs} (left) with the 1:1 line in red; the green points are the values for wavelengths from 660 to 715 nm. Distribution of the relative error between simulated and estimated remote sensing reflectances.

The spectral shape of the remote sensing reflectance is shown in Fig. 14 in the same way as explained for the irradiance reflectance. Two graphs are included in the figure, one for a subsurface viewing angle of $\theta_v = 7^\circ$ and one for $\theta_v = 27^\circ$. The calculated values of the remote sensing reflectance agree very well with the simulations. The relative error is below 5% except for situation number 3, where the error is about 10% around 600 nm. The reason for the discrepancies is the same as for the irradiance reflectance, namely gelbstoff fluorescence.

4. Conclusions

New parameterizations of the irradiance reflectance and the remote sensing reflectance in deep and shallow waters were developed using only the inherent optical properties of the water, the viewing and solar zenith angle, and the surface wind speed. Additionally, a new parameterization for the upward diffuse attenuation coefficient was developed. The new model separates the dependences on inherent optical properties, wind speed, viewing, and solar zenith angle. Thus, their influences can be analyzed very easily. The irradiance reflectance and remote sensing reflectance can be calculated much faster using the analytical equations than with Hydrolight or Monte Carlo methods. The estimations of the irradiance reflectance and remote sensing reflectance agree significantly better with the simulations of Hydrolight than estimations with

#3022 - $15.00 US
Received September 17, 2003; Revised October 23, 2003

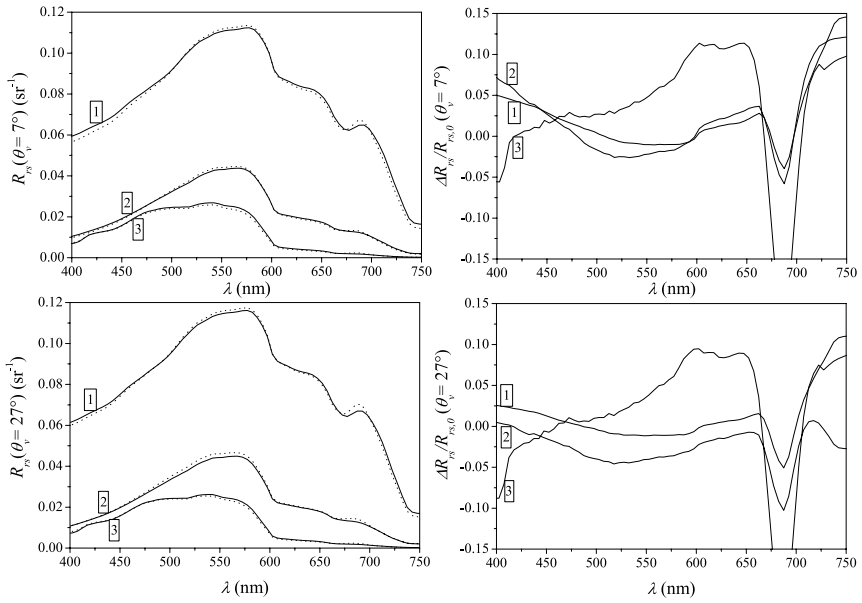

Fig. 14. Remote sensing reflectance of shallow water for the spectral range from 400 to 750 nm for three different cases and for a subsurface viewing angle of $\theta_v = 7°$ on the top and $\theta_v = 27°$ on the bottom. The left part shows the comparison of simulated (dotted lines) and estimated values (solid lines) and the right side the relative errors. The numbers refer to the following situations: (1) sediment at $z_B = 5$ m, $C_P = 10.8$ μg/l, $C_X = 50.0$ mg/l, $a_Y(440\text{nm}) = 0.2$ m^{-1}, $\theta_s = 27°$, $u = 1$ m/s; (2) macrophytes at $z_B = 6$ m, $C_P = 2.5$ μg/l, $C_X = 7.0$ mg/l, $a_Y(440\text{nm}) = 0.3$ m^{-1}, $\theta_s = 33°$, $u = 0$ m/s; (3) sediment at $z_B = 5$ m, $C_P = 1.0$ μg/l, $C_X = 1.0$ mg/l, $a_Y(440\text{nm}) = 0.05$ m^{-1}, $\theta_s = 27°$, $u = 1$ m/s.

existing equations. The mean error is about 2-3%. A maximum error of about 15% occurs at a wavelength of 685 nm owing to the fluorescence of chlorophyll which is not included in the system of equations presented here. The spectral shape of the simulations with Hydrolight fits very well with the new parameterizations. The relative error at a given wavelength is below 5% for the irradiance reflectance and below 10% for the remote sensing reflectance from 400 to 750 nm. Main error sources are the fluorescence of chlorophyll and gelbstoff.

Seasonal changes of the specific optical properties of the water constituents of Lake Constance were investigated previously. The variability of the specific absorption of phytoplankton was analyzed by [19]. He has separated five different algae classes, which allow to model changes of the optical properties of phytoplankton in deep water from 1990 through 1992. The impact on reflectance spectra is small compared to concentration changes. The specific backscattering of suspended matter was determined by [8]. He observed an accuracy of about 25% for the estimated concentration of suspended matter from airborne remote sensing data compared to in situ measurements, indicating a low variability of the specific backscattering coefficient of suspended matter. The gelbstoff exponent S varies about 8% after [22].

With the new parameterizations a set of equations was found for case-2 waters, like Lake Constance. This improves upon existing equations for determining the concentration of the water constituents, bottom depth, and bottom types using by inversion techniques. The analytical

#3022 - $15.00 US Received September 17, 2003; Revised October 23, 2003

equations provide a fast method to process a large set of remote sensing data from hyperspectral airborne and spaceborne sensors. The next step is to implement analytical equations of the fluorescence of chlorophyll and gelbstoff and to test the equations using an independent dataset from Lake Constance and other locations. Inclusion of surface effects and bidirectional bottom effects are also planned.

Acknowledgments

This work is part of the Special Collaborative Program SFB 454 “Lake Constance littoral” funded by the German Research Foundation DFG. Author C.D. Mobley was supported by the Environmental Optics Program of the U. S. Office of Naval Research. Thanks to Peter Gege and Thomas Heege for very constructive comments and suggestions.

#3022 - $15.00 US Received September 17, 2003; Revised October 23, 2003